A Kinetic Study of the Reactions of Sulfate Radicals at the Silica Nanoparticle−Water Interface

Paula Caregnato,[†] Verónica C. Mora,[†] Galo Carrillo Le Roux,[‡] Daniel O. Mártire,*[,†,§] and Mónica C. Gonzalez*[,†,⊥]

Instituto de Investigaciones Fisicoquímicas Teóricas y Aplicadas (INIFTA), Facultad de Ciencias Exactas, Universidad Nacional de La Plata, C. C. 16, Suc. 4, (1900) La Plata, Argentina, and Escola Politecnica da USP−Departamento de Engenharia Quimica, São Paulo, Brasil

Received: October 26, 2002; In Final Form: March 28, 2003

Sulfate radicals, $SO_4^{\bullet-}$, were generated using flash photolysis of aqueous $S_2O_8^{2-}$ solutions and the reactions of the inorganic radicals with the surface of suspended silica nanoparticles (NP) investigated. In the presence of colloidal silica no absorption traces due to $SO_4^{\bullet-}$ radicals are observed at 100 μs after the flash of light. However, two transient species with absorption maxima around 320 and 600 nm are formed. A kinetic analysis of the experimental results indicate that $SO_4^{\bullet-}$ radicals are adsorbed on the NP surface, leading to the formation of an adduct, with $\lambda_{max} \approx 320$ nm ($\epsilon \approx 7000$ cm^{-1} M^{-1}), and showing similar reactivity to that observed for the sulfate radical in aqueous solutions. The NP−sulfate radical adducts react with adsorbed water, and with single and geminal SiO^- sites with reaction rate constants of $1.5 \times 10^{14} \times e^{-(58\pm12)\text{kJ/mol}/RT}$ s^{-1}, $< 10^3 \times e^{-(2\pm17)\text{kJ/mol}/RT}$ s^{-1} and $< 10^{11} \times e^{-(46\pm13)\text{kJ/mol}/RT}$ s^{-1}, respectively. Two different $SiO^\bullet$ surface defects, showing similar spectra ($\lambda_{max} \approx 600$ nm) but different reactivities, are formed from the reaction of NP−sulfate radicals and deprotonated geminal and single silanols.

Introduction

Silica is one of the most common materials on earth. The surface properties of liquid/silica interfaces and the role played by the silica surface in interfacial chemical kinetics are important to understand processes involved in catalysis,[1] environmental chemistry,[2a] in particular soil chemistry,[2b] and chromatography.[3,4]

Amorphous silica surfaces can be described by the Zhuralev model,[5] which considers that the factor determining the surface properties is the presence of silanol groups and siloxane bridges. Chemical reactions involving the latter moieties lead to modifications of the surfaces, which may be used, on one hand, to provide information on the structure of the silica surface, such as nanorugosity, chemical fractality, and distribution of surface silanols.[5] On the other hand, the chemical reactivity of the surface active groups can be used to yield a solid surface with entirely different properties (hydrophobic materials, functionalized derivatives, etc.).[6]

Silica immersed in an aqueous environment has been shown to orient its surface silicon atoms in a tetrahedral configuration with each Si atom holding approximately one OH group.[5] A total of 4.6−4.9 OH groups per nm^2 is found for all types of fully hydroxylated silica, independent of its origin.[5] Single, $(\equiv Si-O-)_3Si-OH$, and geminal, $(\equiv Si-O-)_2Si(-OH)_2$, silanols present in an irregular arrangement, act as centers of adsorption of molecules capable of forming H bonds or of undergoing donor−acceptor interactions. Dissociation of surface hydroxyl groups to SiO^- ions renders a negatively charged silica surface.[7] A number of different studies carried out on aqueous suspensions of silica or with macroscopic silica,[8−15] indicate that there are at least two types of silanol groups at the water/silica interface characterized by a dissociation pK_a of 4.5−6.5 for about 15% of the silanol sites and a pK_a value of 8.5−9.0 for the remaining 85%. The pK_a values of 4.5−6.5 and 8.5−9.0 were associated with the geminal and single silanols, respectively.[16,17]

An experimental approach employed here to study liquid/solid interfaces involves colloidal particles dispersed at modest concentrations which provide a high concentration of surface sites for reaction. Since colloidal silica has a very high specific surface area and is optically transparent in the near-UV and visible regions, it is a suitable model surface for investigating interfacial reaction kinetics involving photochemically generated species. As a result, sulfate radicals, $SO_4^{\bullet-}$, were generated using flash photolysis ($\lambda > 200$ nm) of aqueous $S_2O_8^{2-}$ solutions,[18,19] reaction R1. Then the reactions of the inorganic radicals with the silica nanoparticle (NP) surface were investigated following the radical production.

$$S_2O_8^{2-} + h\nu \rightarrow 2SO_4^{\bullet-} \qquad \text{(R1)}$$

Experimental Section

Sodium peroxodisulfate (p.a.), sodium perchlorate (99%), perchloric acid (70−72% aqueous solution), sodium hydroxide (99%), and absolute ethanol (99.8%), all from Merck, were used as received. Distilled water (>18 MΩ cm^{-1}, <20 ppb of organic carbon) was obtained from a Millipore system.

For most experiments stock Ludox colloidal silica suspensions (SM-30, 30 wt % SiO_2 in water at pH 10.2 with an average particle diameter of 7 nm, surface area: 345 m^2/g, Aldrich) were used. For some experiments colloidal silica was obtained by

* To whom correspondence should be addressed.
† Universidad Nacional de La Plata.
‡ Escola Politecnica da USP−Departamento de Engenharia Quimica.
§ E-mail: dmartire@inifta.unlp.edu.ar.
⊥ E-mail: gonzalez@inifta.unlp.edu.ar.

10.1021/jp027318t CCC: $25.00
Published on Web 05/31/2003

suspending fumed silica nanoparticles (silica content, 99.8%; surface area, 390 ± 40 m^2/g; particle diameter, 7 nm; Sigma) in aqueous solutions.

The pH of the samples was measured with a Methrom-Herisau pH meter model E512. Ludox colloidal silica dilutions to concentrations of the order of 0.025 mg/mL yields dispersions of pH 8.0−8.4. Since silica sols at pH 8 were reported to remain stable even in the presence of salt concentrations of the order of 0.15 M,[20] this pH was used in most experiments. When required, the samples were acidified with $HClO_4$. Ludox colloidal silica has its greatest tendency to gel at pH 5−6, and consequently this pH range was avoided. At lower pH, sols become more stable. Colloidal dispersions of pH > 10.5 were not used because (i) an efficient scavenging of sulfate radicals by HO^- ions takes place[21] and (ii) in this pH range colloidal silica becomes increasingly solubilized and the alkali silicate thus formed destabilizes the remaining colloids.

Because of the reduction in sol stability by added salts, the ionic strength of the nanoparticle suspensions was not adjusted, except otherwise indicated. When necessary, the ionic strength was varied by addition of sodium perchlorate up to values ≤0.15 M because of sol stability.

The NP concentration used was in the range 0.00025−0.25 g/L. Higher values were avoided, since flash photolysis experiments of persulfate solutions using increasing NP concentrations in the water-jacket around the flash cell, show that high concentrations of NP act as a filter to the absorption of light by $S_2O_8^{2-}$ ions. The light intensity emerging from samples of persulfate in the absence and presence of NP was coincident for NP concentrations < 0.25 g/L, λ > 300 nm, and an optical path length of 20 cm. Therefore, any interference by scattered light is of no significance under the experimental conditions used in the photolysis experiments.

In experiments with ethanol, [EtOH] ≥ 2×10^{-5} M was used because of the requirement $[SO_4^{\bullet-}]_0 \ll$ [EtOH] such that the ethanol concentration remains constant throughout the experiment. The upper limit [EtOH] ≤ 1×10^{-4} M was chosen in order to minimize the contribution of the competing reaction of ethanol with sulfate radicals.

Flash-photolysis experiments were carried out with a conventional apparatus [22] (Xenon Co. model 720C) with modified optics and electronics.[23] Two collinear quartz Xenon high-intensity micropulse flash tubes, Xenon Corp. P/N 890−1128 (fwhm ≤ 20 μs), with a continuous spectral distribution ranging from 200 to 600 nm and maximum around 450 nm were used. The analysis source was a high-pressure mercury lamp (Osram HBO-100 W). The optical path length of the 1 cm -internal diameter quartz sample cell was 20 cm. The monochromator collecting the analysis beam (Bausch & Lomb, high intensity) was coupled to a photomultiplier (RCA 1P28), whose output was fed into a digital oscilloscope (Leader LBO-5825). Digital data were stored in a personal computer. The temperature was controlled to ±0.5 K by circulating distilled water from a thermostat model NB-D8/17 MGW-Lauda, through the jacket of the reaction cell. The temperature was measured inside the reactor cell with a calibrated Digital Celsius Pt-100 Ω thermometer.

Bilinear Regression Analysis. For each experimental condition, several absorbance decay profiles at different detection wavelengths were taken. Absorbance is thus a function of wavelength and time. A bilinear regression analysis taking advantage of the linearity of the absorbance with both concentrations and absorption coefficients, was applied to the experimental absorption matrix in order to retrieve information on the minimum number of species and on their relative concentration profiles and absorption spectra.[24]

The absorbance may be written in a matrical form $[\mathbf{a}] = [\epsilon][\mathbf{c}]$, where $[\mathbf{a}]$, $[\epsilon]$, and $[\mathbf{c}]$ represent the absorbance, absorption coefficients, and concentrations matrixes, respectively. The procedure is based on the alternating calculus of the matrices $[\epsilon]$ and $[\mathbf{c}]$ by multiple linear regression (using a least-squares condition) iteratively until convergence is achieved when the elements of an error matrix are minimized. From the error matrix, a corrected absorbance matrix, $[\mathbf{a}^c]$, is obtained. The number of species is selected as the minimum value that allows a reasonable approximation between $[\mathbf{a}^c]$ and $[\mathbf{a}]$.

Kinetic Computer Simulations. The kinetic model for computer simulation is based on component balances and equilibrium equations formulated in terms of a differential algebraic equations system which is solved by Gear's Stiff method and a least-squares estimation criterion.[25] The version implemented performs the solution of the differential algebraic equations system concomitantly to the evaluation of the parametric sensitivities based on the decoupled direct method. In consequence, the simulation of the system is robust, such that it can be carried out with success for very different parameter values, while the sensitivities are accurate and obtained without much computational effort. The algorithm for minimization criterion is based on the rotational discrimination and provides additional features for assessing the identifiability of the problem.

Global Analysis. The algorithm employed for the computer simulations (vide supra) was used as a criterion for the goodness of the fit to a given function and to obtain the best kinetic parameters (weight coefficients and rate constants) describing the absorbance profiles of a group of experiments obtained at different λ and under different experimental conditions.

Results and Discussion

The $SO_4^{\bullet-}$ radical ions were generated by photolysis (λ > 200 nm) of $(2-7) \times 10^{-3}$ M peroxodisulfate solutions[19,26] in the pH range 3−9, reaction R1. In the absence of colloidal silica, the transient absorption spectrum and the decay rate were coincident with those reported for $SO_4^{\bullet-}$ radicals.[19] Figure 1, lower inset, shows the signals obtained at 450 nm after photolysis of 1×10^{-3} M $S_2O_8^{2-}$ solutions. Flash photolysis of colloidal silica dispersions in the absence of peroxodisulfate showed, within our experimental error, no transient absorption.

Flash photolysis of aqueous $(2-7) \times 10^{-3}$ M peroxodisulfate containing (0.00025−0.25) g/L colloidal silica, shows no absorption traces due to $SO_4^{\bullet-}$ radicals in our time window ($t \geq 100$ μs). However, absorption traces with maxima at around 320 nm (Figure 1) and 600 nm (Figure 1, upper inset) with markedly different decay kinetics are observed, indicating the presence of at least two absorbing species. The traces adsorbing in the wavelength range from 480 to 680 nm are formed with the same rate as the transient with $\lambda_{max} \approx 320$ nm decays (see Figure 1).

The decay kinetics and absorption spectra of both transients were found to be independent, within the experimental error, of the presence of dissolved molecular oxygen in the range $0 < [O_2] < 2.5 \times 10^{-4}$ M. Therefore, most experiments were performed with air-saturated suspensions. The pH decreases with the number of flashes irradiated on the samples and consequently, freshly prepared solutions were used for all experiments. A good reproducibility of the transient signals is observed for all the experimental conditions.

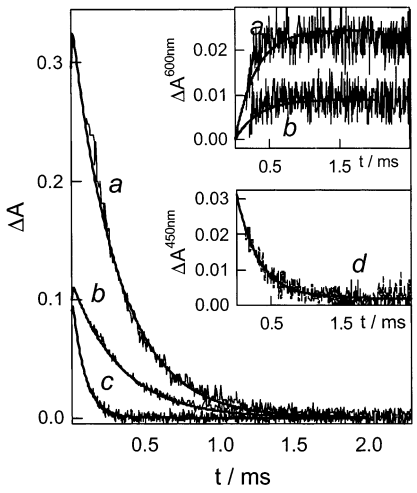

Figure 1. Absorbance profiles obtained at 320 nm for experiments with 0.025 g/L NP (Ludox), pH = 8 and (a) 5×10^{-3} M $S_2O_8^{2-}$ at 285.2 K, (b) 1×10^{-3} M $S_2O_8^{2-}$ at 285.2 K, and (c) 1×10^{-3} M $S_2O_8^{2-}$ at 298.2 K. Upper inset: Absorbance profiles obtained at 600 nm for experiments a and b of the main figure. Lower inset: Curve d, corresponding to the absorbance profile obtained at 450 nm for experiments with 1×10^{-3} M $S_2O_8^{2-}$ at 298.2 K in the absence of added NP. Solid curves represent computer simulations (refer to text).

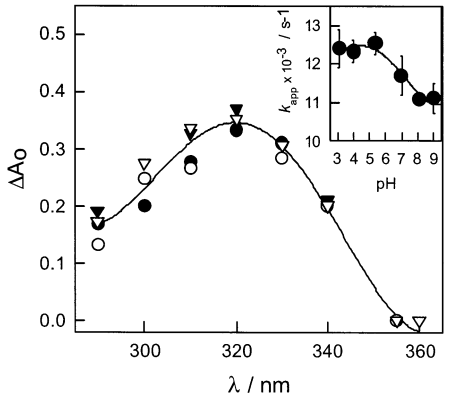

Figure 2. Absorption spectrum of the transient with λ_{max} around 320 nm for experiments at 298.2 K with 0.025 g/L NP (Ludox) suspensions containing 5×10^{-3} M $S_2O_8^{2-}$ at pH (●) 3.0, (▼) 4.0, (○) 7.0, and (▽) 9.0. Inset: Plots of k_{app} vs pH for the experiments in the main figure.

Experiments performed with nanoparticles of different origin (Sigma and Ludox suspensions) but otherwise identical experimental conditions, qualitatively show the same behavior. For quantitative analysis, experiments were mainly performed with Ludox NP suspensions.

For clarity, the behavior of both observed transients is described separately.

Transient with Absorption Maximum around 320 nm. Time-resolved absorption curves were obtained from experiments performed with 1×10^{-3} M $\leq [S_2O_8^{2-}] \leq 5 \times 10^{-2}$ M, 0.00025 g/L $\leq$ [NP] $\leq$ 0.25 g/L, and pH in the range from 3 to 9. For each colloidal dispersion, several absorbance decay profiles were taken at different detection wavelengths within the range 290−360 nm. For all the experimental conditions used, the bilinear regression analysis applied to the absorbance matrix (see Experimental Section) shows that the data may be described by only one absorbing species.

The absorption spectrum of the observed transient is independent of pH in the range from 3 to 9 (see Figure 2). The decay rate of the transient follows a first order kinetics with a rate constant slightly decreasing with increasing pH (see Figure 2 (inset)).

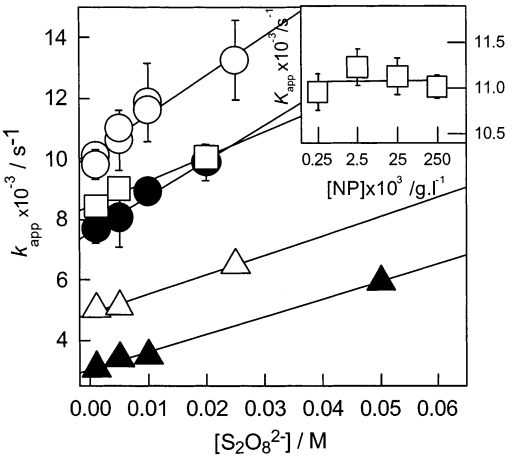

Figure 3. Dependence of k_{app} with $S_2O_8^{2-}$ concentration for experiments with suspensions of pH 8 and 0.025 g/L NP (Ludox) at 285.6 (▲), 288.7 (△), 293.2 (●), and 298.4 K(○). Open squares correspond to samples of pH = 4.2 at 293.2 K. Unless otherwise indicated, error bars in k_{app} are of the order of the symbol size. Inset: Dependence of k_{app} with NP concentration for experiments with suspensions of pH 8 and 5×10^{-3} M $S_2O_8^{2-}$ at 298.4 K

Experiments with samples of pH = 8 containing 5×10^{-3} M $S_2O_8^{2-}$ and various NP concentrations showed transient decay rates with pseudo first-order rate constant, k_{app}, independent of [NP] (see Figure 3 (inset)). The initial absorption of the transient was also found to be independent of [NP], except for [NP] = 0.25 mg/mL which shows lower initial absorbance due to an internal filter effect (vide supra).

Irradiation of samples of variable ionic strength in the range from 3×10^{-3} to 0.15 M, pH = 8, 0.025 g/L NP, and $[S_2O_8^{2-}] = 10^{-3}$ M at 293.2 K yields traces which, within the experimental error, show identical decay rate constants and initial absorbance (results not shown). For colloidal dispersions with $[S_2O_8^{2-}] = 2 \times 10^{-2}$ M, variations of the ionic strength were limited to the range 0.06 to 0.15 M. Under such conditions, no ionic strength effect on the decay rate was observed within the experimental error. Therefore, variations in the ionic strength up to values $\leq$ 0.15 M is of no significance for the decay of the transient.

Experiments with samples of pH = 8 containing 0.025 g/L NP and various $S_2O_8^{2-}$ concentrations showed faster transient decay rates with increasing $[S_2O_8^{2-}]$ (see Figure 1). The traces could be well fitted to a first-order kinetics with a pseudo first-order rate constant, k_{app}, linearly increasing with $[S_2O_8^{2-}]$, as shown in Figure 3 for different temperatures in the range 285 to 299 K and also for colloidal dispersions of pH 4 at 293.2 K. Figure 4 shows the Arrhenius plots of the intercepts, *a*, and slopes, *b*, of the straight lines in Figure 3 (except for that at pH 4), yielding activation energies of 58 ± 12 and 53 ± 15 kJ/mol, respectively.

The initial absorption of the transient increases with $S_2O_8^{2-}$ concentration, as shown in Figure 1 for $[S_2O_8^{2-}] = 1 \times 10^{-3}$ and 5×10^{-3} M at 285.2 K. A similar behavior is observed for initial sulfate radical concentrations, formed by reaction R1 in experiments in the absence of NP but under otherwise identical experimental conditions, as expected for the dependence of the absorbed light intensity on $[S_2O_8^{2-}]$. These observations further support that formation of the transient absorbing at these wavelengths is intimately related to sulfate radical generation from reaction R1.

Moreover, for each $[S_2O_8^{2-}]$, the initial absorption of the traces may be assumed to be, within the 20% error dispersion,

TABLE 1: Reaction Manifold of $SO_4^{\bullet-}$−NP Adducts[a]

	rate constant	activation energy	
$SO_4^{\bullet-} + NP \rightarrow NPS^{\bullet}$	$k_2 \geq 1 \times 10^7\ s^{-1}\ m^{-2}$		(R2)
$NPS^{\bullet} + S_2O_8^{2-} \rightarrow$	$k_3 = (1.3 \pm 0.2) \times 10^5\ M^{-1}\ s^{-1}$	$E_{a3} = (53 \pm 15)$ kJ/mol	(R3)
$NPS^{\bullet} \rightarrow$	$k_4 = (1.01 \pm 0.02) \times 10^4\ s^{-1}$		(R4)
$NPS^{\bullet} + C_2H_5OH \rightarrow$	$k_5 = (3.1 \pm 0.2) \times 10^7\ M^{-1}\ s^{-1}$		(R5)

[a] Depicted values correspond to colloidal suspensions of pH = 8 at 298 K.

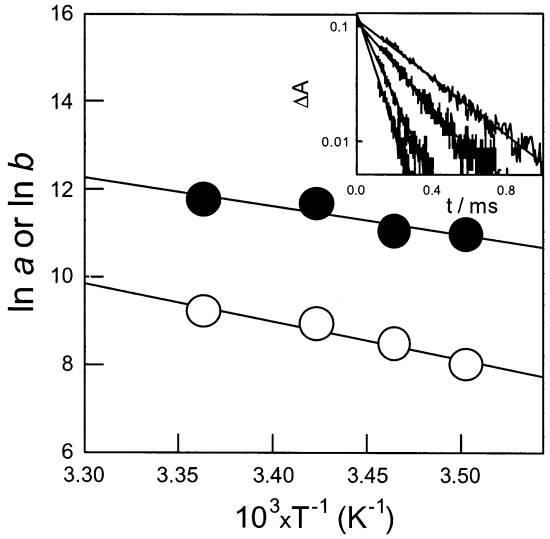

Figure 4. Arrhenius plots of intercept a (○) and slope b (●) of the lines in Figure 3, except for that at pH = 4.2. Error bars in k_{app} values are of the order of the symbol size. Inset: Absorbance profiles obtained at 320 nm for experiments with 0.025 g/L NP (Ludox) and 1×10^{-3} M $S_2O_8^{2-}$ at pH = 8 and, from bottom to top: 298.4, 293.2, 288.7, and 285.9 K. The solid lines stand for first-order fits.

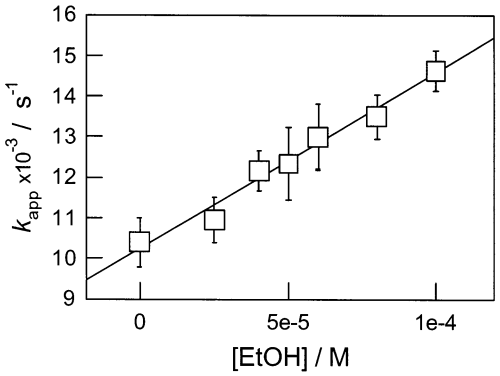

Figure 5. Plot of k_{app} vs ethanol concentration for experiments at 298.7 K with [NP (Ludox)] = 0.025 g/L, $[S_2O_8^{2-}] = 5 \times 10^{-3}$ M and pH 8. The error bars represent standard deviations.

independent of temperature as shown by the intercepts of the first-order plots in Figure 4 (inset). The quantum yield (Φ_1) of sulfate radical formation by reaction R1, and the reciprocal of the $SO_4^{\bullet-}$ lifetime increase with increasing temperature.[27] Thus, the two opposite effects on the amounts of transient formed by reaction R2 result in the constant initial concentration of the observed transient, which supports a global small activation energy for this reaction.

Experiments performed at 298.7 K with 0.025 g/L NP suspensions of pH = 8 containing 5×10^{-3} M $S_2O_8^{2-}$ in the presence of various amounts of ethanol, showed transient decay rates which followed a first-order kinetics with k_{app} linearly increasing with [EtOH] (see Figure 5). The slope and the intercept of the straight line in Figure 5 obtained form a least-squares analysis are $(4.5 \pm 0.3) \times 10^7\ s^{-1}\ M^{-1}$ and $10\,100 \pm 200\ s^{-1}$, respectively. The error bars for these rate constants and for all other data reported here are the standard deviations, σ.

The observed results indicate that the transient with λ_{max} around 320 nm, denoted as $NPS^{\bullet}$, is formed after the interaction of $SO_4^{\bullet-}$ radicals with the nanoparticle surface, reaction R2. The $SO_4^{\bullet-}$ radicals are depleted within less than 100 μs by NP concentrations as low as 0.00025 g/L and a total surface area of 0.00135 m^2 in the reaction cell. Therefore, k_2 is $\geq 1 \times 10^7\ s^{-1}\ m^{-2}$ for the reaction of sulfate radical with the silica surface.

The most simple mechanism explaining the observed trends for the decay of $NPS^{\bullet}$ in the absence of ethanol considers reactions R2−R4 in Table 1, with a first-order apparent rate constant $k_{app} = k_4 + k_3[S_2O_8^{2-}]$, as expected from the observed dependence of k_{app} on $[S_2O_8^{2-}]$, vide supra. The observed transient is also able to react with ethanol as depicted in reaction R5.

The pH independent spectrum and initial concentration of $NPS^{\bullet}$ indicate that $NPS^{\bullet}$ does not take part of an acid/ base equilibrium and that $NPS^{\bullet}$ formation is not due to a chemical reaction between $SO_4^{\bullet-}$ radicals and surface silanols. Otherwise, differences in the spectrum and initial absorption would arise within the pH range from 3 to 9, as the pK_a of the silanol sites were reported to be within this range,[12] vide supra.

Both the reactions of $NPS^{\bullet}$ with peroxodisulfate and ethanol, reactions R3 and R5, show rate constants of the same order of magnitude as those reported for the sulfate radicals with these substrates in aqueous solutions ($k = 6 \times 10^5\ M^{-1}\ s^{-1}$ and $5 \times 10^7\ M^{-1}\ s^{-1}$, respectively).[28] This observation seems to indicate that $NPS^{\bullet}$ chemically behaves like a sulfate radical. Identification of the $NPS^{\bullet}$ transient with a $SiO^{\bullet}$ or $SiOO^{\bullet}$ radical on the NP surface, may be neglected, since these radicals were reported to absorb around 630 and 230 nm, respectively.[29] Moreover, $SiO^{\bullet}$ reactivity would resemble that of the silicate radical, $SiO_3^{\bullet-}$, which shows a much lower rate constant for its reaction with ethanol[28] ($k = 8.3 \times 10^5\ M^{-1}\ s^{-1}$) than that observed for reaction R5. Formation of silicon radicals, $Si^{\bullet}$, may also be neglected, since these radicals are efficiently quenched by molecular oxygen,[29] contrary to our results showing no effect with the dissolved [O_2]. Therefore, $NPS^{\bullet}$ may be assigned to a NP−sulfate adduct, as also supported by a low activation energy for reaction R2.

No effect of the ionic strength on the decay rate of $NPS^{\bullet}$ was observed for experiments with $[S_2O_8^{2-}] = 10^{-3}$ M, where mainly reaction R4 contributes to transient depletion. The latter observation indicates that reaction R4 should be, either a chemical reaction between uncharged substrates or a surface process between adsorbed molecules.

The surface reaction of $NPS^{\bullet}$ with adsorbed water (reaction R4a in Table 2) yields H^+, in agreement with the pH decrease observed after flash irradiation. A similar reaction is observed in aqueous solutions between sulfate radicals and water molecules.[28] Reaction of $NPS^{\bullet}$ with surface silanols, SiOH, or with their conjugate base, SiO^-, as shown in reaction R4b for the latter groups, should also be considered. Both, an H− abstraction of $NPS^{\bullet}$ radicals from surface silanols or an electron-transfer

TABLE 2: Detail of the Surface Reactions R4 of the NP−Sulfate Adduct[a]

	activation energy (kJ/mol)	preexponential factor (s^{-1})	
$[NPS^{\bullet} + H_2O(ads)]_{surface} \rightarrow NP + HO^{\cdot} + H^+$	58 ± 12	1.5×10^{14}	(R4a)
$[NPS^{\bullet} + >Si(-O^-)_2]_{surface} \rightarrow >Si(O^-)O^{\bullet} + SO_4^{2-}$	46 ± 13	$<1 \times 10^{11}$	(R4bg)
$[NPS^{\bullet} + \gtrdot Si-O^-]_{surface} \rightarrow \gtrdot Si-O^{\bullet} + SO_4^{2-}$	2 ± 17	$<1 \times 10^{3}$	(R4bs)

[a] Depicted values correspond to suspensions of pH = 8. The characters g and s stand for geminal and single silanols, respectively.

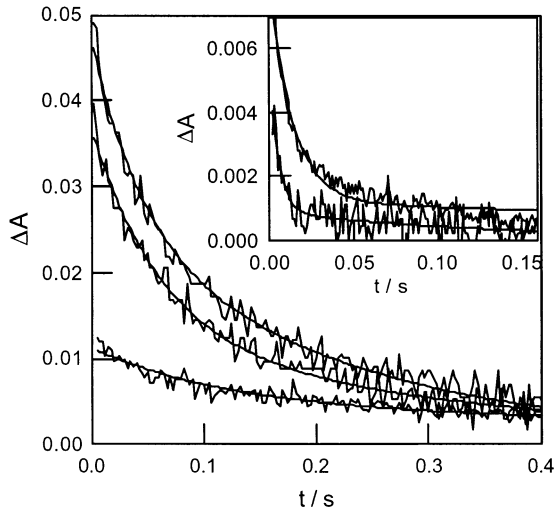

Figure 6. Absorbance profiles obtained at 600 nm for experiments with 0.025 g/L NP (Ludox), pH 8 and (from bottom to top) 1×10^{-3}, 4.5×10^{-3}, and 7×10^{-3} M $S_2O_8^{2-}$. Inset: Absorbance profiles obtained at 600 nm for experiments with 0.025 g/L NP (Ludox), pH = 8 and 5×10^{-3} M $S_2O_8^{2-}$ in the presence of 2×10^{-5} M (lower trace) and 5×10^{-5} M ethanol. These experiments were performed at much lower light intensities than those in the main figure. The solid lines stand for a global computer analysis (see text).

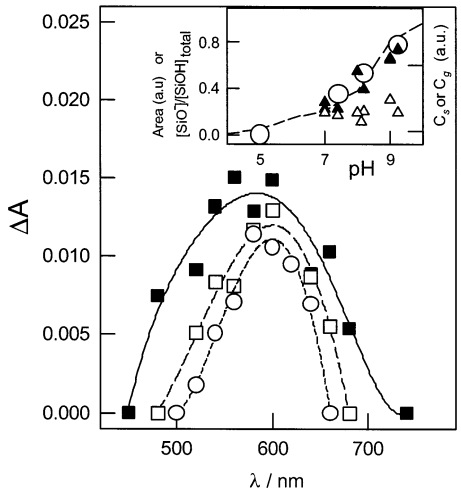

Figure 7. Absorption spectrum of the transient with maximum around 600 nm for experiments with $[S_2O_8^{2-}] = 2.7 \times 10^{-4}$ M and [NP (Sigma)] = 0.00025 g/L at different pH: (■) 9.2, (□) 8.2, and (○) 7.4. Inset: pH dependence: (○) the area below the curves in the main figure, (△) C_g, and (▲) C_s, all in arbitrary units. The solid lines stand for the fraction of dissociated silanols, $[SiO^-]/[SiOH]_{total}$ vs pH.

process between $NPS^{\bullet}$ and SiO^-, reaction R4b, yield surface $SiO^{\bullet}$ radicals.

Transient with Absorption Maximum around 600 nm. Transient formation at 600 nm is fast (half time $<1.5 \times 10^{-4}$ s^{-1}) compared to its decay rate (half time on the order of 0.01 s^{-1}), as shown by the traces in Figures 1 (inset) and 6. Therefore, the formation and decay kinetics of the transient may be independently analyzed.

Under all the experimental conditions used, the decay of the traces in this wavelength range may be well fitted to a biexponential function, eq 1. In this equation the subscripts s and g stand for the slow and fast decaying components, respectively.

$$\Delta A = C_g e^{-k_g t} + C_s e^{-k_s t} \quad (1)$$

The transient absorption decreases with pH in the range from 9 to 6 and no signal is observed below pH 5.4 (see Figure 7). The biexponential analysis of the traces yield k_g and k_s values which are, within error, independent of the detection wavelength and pH. The coefficients C_g and C_s are wavelength- and pH−dependent. The general behavior observed for each given wavelength indicates an increase in C_s and constant C_g values with increasing pH (see Figure 7 (inset)).

Experiments in the temperature range from 284 to 301 K show increasing decay rates and decreasing signal amplitudes with increasing temperature. Arrhenius plots for k_g and k_s (see Figure 8) obtained for experiments with 1×10^{-3} M $S_2O_8^{2-}$ and 0.025 g/L NP suspensions of pH = 8 yield global activation energies $E_g = 30 \pm 11$ and $E_s = 39 \pm 16$ kJ/mol, respectively. Both C_g and C_s decrease at higher temperatures (see Figure 8 (inset)).

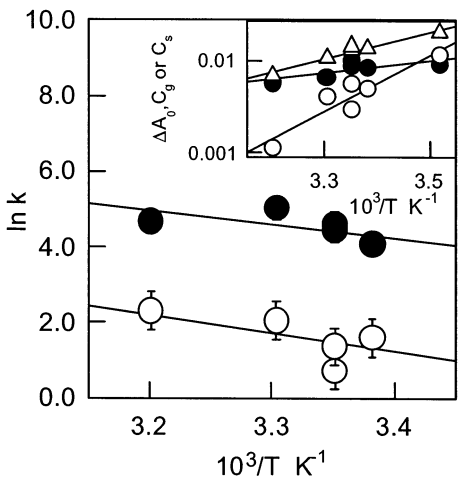

Figure 8. Arrhenius plot of k_s (○) and k_g (●) for experiments with [NP (Ludox)] = 0.025 g/L at pH 8 and $[S_2O_8^{2-}] = 1 \times 10^{-3}$ M. Unless otherwise indicated by the corresponding bars, the error in ln k values are of the order of the symbol size. Inset: Logarithm plots of C_s (○), C_g (●), and ΔA_0 (△) obtained at 600 nm vs the inverse of the temperature for the experiments in the main figure.

Experiments with dispersions of pH = 8 containing 5×10^{-3} M $S_2O_8^{2-}$ and various [NP] in the range from 0.25 to 0.0025 g/L showed transient decay rates with pseudo first-order rate constants k_g and k_s linearly increasing with [NP] (not shown). The absolute rate constant for the reactions of the fast and slow transients with NP are $(1.9 \pm 0.2) \times 10^7$ and $(1.5 \pm 0.8) \times 10^6$ M^{-1} s^{-1}, respectively. The coefficients C_g and C_s were found to be independent of [NP].

Experiments with various initial $[S_2O_8^{2-}]$ but otherwise identical experimental conditions, showed faster transient decay rates and higher absorbance with increasing $[S_2O_8^{2-}]$ (see Figure 6). The latter observation is in agreement with the behavior

TABLE 3: Manifold of Reactions of SiO• Surface Defects[a]

	rate constant (M^{-1} s^{-1}) for SiO• generated from geminal SiO^-	rate constant (M^{-1} s^{-1}) for SiO• generated from single SiO^-	
$SiO^\bullet + NP \rightarrow$	$k_{6g} = (1.9 \pm 0.2) \times 10^7$	$k_{6s} = (1.5 \pm 0.8) \times 10^6$	(R6)
$SiO^\bullet + S_2O_8^{2-} \rightarrow$	$k_{7g} = 2500 \pm 300$	$k_{7s} = 630 \pm 50$	(R7)
$SiO^\bullet + C_2H_5OH \rightarrow$	$k_{8g} = (3.5 \pm 1) \times 10^6$	$k_{8s} = (8 \pm 5) \times 10^4$	(R8)

[a] Depicted values correspond to suspensions of pH = 8 at 298 K.

expected for the 600 nm transient formed from the decay of NPS•. Fit is obtained from a least-squares analysis to eq 1, and the results give k_g and k_s. The k_g and k_s values are found to be linearly dependent on the $S_2O_8^{2-}$ concentration.

Data obtained from suspensions of pH = 8 containing 0.025 g/L NP and 5×10^{-3} M $S_2O_8^{2-}$ and different ethanol concentrations in the range $(1-10) \times 10^{-5}$ M, showed faster decay kinetics with increasing ethanol concentrations (see Figure 6 (inset)). Fit is obtained from a least-squares analysis to eq 1, and the results give k_g and k_s. The k_g and k_s values are found to be linearly dependent on the EtOH concentration. The amount of transient formed decreases with increasing ethanol concentration, in agreement with a transient precursor which is also reactive toward ethanol, as is the case of NPS•.

The previous results indicate that the observed traces are due to two transient components, both reacting with NP, $S_2O_8^{2-}$, and ethanol as shown in reactions R6−R8 in Table 3, where SiO• stands for the transients absorbing at 600 nm. The overall decay rate constants k_g and k_s are those depicted in eqs 2a and 2b, respectively.

$$k_g = k_{6g}[NP] + k_{7g}[S_2O_8^{2-}] + k_{8g}[EtOH] \quad (2a)$$

$$k_s = k_{6s}[NP] + k_{7s}[S_2O_8^{2-}] + k_{8s}[EtOH] \quad (2b)$$

A computer global analysis of the traces observed in the wavelength range 560−640 nm for experiments with [NP] = 0.025 g/L, pH = 8, 10^{-3} M $\leq [S_2O_8^{2-}] \leq 2 \times 10^{-2}$ M and $0 \leq [EtOH] \leq 1 \times 10^{-4}$ M, at 298.2 K, was used in order to retrieve the values of the absolute rate constants in eqs 2a and 2b with minimized error. The best fitting values are those depicted in Table 3. The goodness of the global analysis is shown by the solid lines in Figure 6. The observed values $k_{6s}[NP] < 0.1$ s^{-1} and $k_{6g}[NP] = 5.4 \pm 0.6$ s^{-1}, are in agreement with the expected values for the reaction of the transients with the NP concentration used (see above), which indicates that a reaction of the transient with water should have a negligible contribution to the overall decay rate of this transient.

The ionic strength (μ) effect was studied in experiments with 2×10^{-2} M $S_2O_8^{2-}$ and 0.025 g/L NP at pH = 8 under conditions where both transient components decay mainly by reaction R7. The decay rate constant for the slow transient component does not depend, within the experimental error, on the ionic strength in the range from 6×10^{-2} M to 0.15 M. However, plots of log k_g vs $\mu^{1/2}/(\mu^{1/2} + 1)$ yield straight lines with a slope value of 1.7 ± 0.3. The observed value is expected for the reaction of two repelling species, $S_2O_8^{2-}$ ions and a negatively charged nanoparticle.

Nonbridging oxygen hole centers assigned to surface SiO• radicals in glassy SiO_2 and SiO_2 nanoparticles show absorption around 630 nm,[29] with a spectrum similar to that reported for $SiO_3^{\bullet-}$ radicals.[30] The transient absorbing in the wavelength range from 480 to 680 nm formed from the NPS• radical may thus be assigned to the surface SiO• radicals. This assignment is also supported by the similar reactivity toward ethanol observed for the 600 nm transient (reaction R8) and that reported for $SiO_3^{\bullet-}$ radicals (vide supra).

Deeper Insight into the Reaction Mechanism. SiO• signals were not observed in suspensions of pH below 5.4, where all surface hydroxyls are in their undissociated form, thus indicating that the reaction between NPS• and surface silanols is of no significance. However, increasing concentrations of SiO• radicals are formed with increasing pH, as the fraction of surface dissociated silanols also increases. Figure 7 (inset) shows the good agreement between the pH dependence of the area below the absorption spectrum of SiO• radicals and the fraction of dissociated silanols at different pH calculated taking the reported[15] pK_a values (vide supra). Therefore, the electron-transfer reaction between surface dissociated silanols and the adsorbed sulfate radical, reaction R4b, is of significance at pH > 5.3. The behavior for NPS• surface reactions with SiO^- and SiOH is similar to that of the reactions of $SO_4^{\bullet-}$ radicals with SiO_3^{2-} ($k = 2 \times 10^7$ M^{-1} s^{-1}) and H_2SiO_3 ($k < 2 \times 10^5$ M^{-1} s^{-1}) in aqueous solutions,[28] as for both systems, the electron-transfer process is more efficient than H-abstraction. The latter observation further stresses the similar reactivity patterns of the NPS• transient and $SO_4^{\bullet-}$ radicals.

The increase in the concentration of SiO• surface radicals with the fraction of total deprotonated silanols indicate that the two types of silanol sites characterized by pK_a of 4.5−6.5 and 8.5−9.0 [8−15,17] participate in reaction R4b. The fast and slow components of the decay rates of the 600 nm transient may thus be related to these two silanol sites as indicated by the pH dependence of the weight factors C_g and C_s. The independence of C_g with pH in the range from 7 to 9 suggests that this component is associated with the silanol site with the lower pK_a, while the increase with pH of C_s follows the increase in the fraction of dissociated silanols due to those sites with pK_a = 8.5−9.0.

Since the two types of silanol groups on the surface of a fully hydroxylated silica have been correlated with isolated and geminal silanols,[16,17] the fast and slow components of the SiO• transient may be assigned to radicals formed from geminal and single SiO^- sites, reactions R4bg and R4bs, respectively. The SiO• surface defects in both sites show identical absorption spectrum. The geminal silanols have been regarded as the reactive sites for adsorption and chemical reaction.[17] We also observe here that SiO• radicals arising from geminal SiO^- are more reactive than those radicals arising from single SiO^-. The measurable ionic strength effect observed for the fast SiO• component may be explained by the proximity of a negative charge due to the dissociated geminal silanol. On the other hand, SiO• radicals arising from single SiO^- have their nearest negative charge at farther distances,[17] and consequently, they are less prone to influence the SiO• reacting center.

For experiments with low $[S_2O_8^{2-}]$, higher SiO• signals were observed to be formed at lower temperatures. Under these experimental conditions, reaction R3 is of no importance and mainly reactions R4a, R4bg, and R4bs compete for the NPS• transient. The total concentration of surface SiO• formed from geminal SiO^- is proportional to C_g. Since the initial concentration of NPS• does not depend on temperature and considering that $k_{4a} > k_{4bg}$, k_{4bs} and k_{4bg} is of the same order of magnitude

than k_{4bs} and an Arrhenius behavior exists for the three competing reactions, eq 3 is obtained.

$$C_g = \frac{A_{4a}}{A_{4bg}} \times \exp\left(\frac{E_{4a} - E_{4bg}}{RT}\right) \quad (3)$$

where *A* stands for the preexponential factors.

A similar dependence is observed for surface $SiO^\bullet$ formed from single SiO^-. In fact, plots of the logarithm of C_g and C_s vs the inverse of the absolute temperature yield straight lines (see Figure 8 (inset)) from which $(E_{4a} - E_{4bg}) = 12 \pm 6$ and $(E_{4a} - E_{4bs}) = 57 \pm 11$ kJ mol^{-1} are obtained. Therefore, the observed temperature dependence for the apparent rate constant $k_4 = k_{4a} + k_{4bg} + k_{4bs}$ is mainly due to reaction R4a and the estimated activation energies are $E_{4a} = 58 \pm 12$ kJ mol^{-1}, $E_{4bg} = 46 \pm 13$ kJ mol^{-1} and $E_{4bs} = 2 \pm 17$ kJ mol^{-1}. The different values observed for E_{4bg} and E_{4bs} indicate different environments as expected for single and geminal dissociated silanols. The reaction of sulfate radicals with water solvent shows an activation energy of 9.2 kJ mol^{-1}.[28] Since physically adsorbed water forms hydrogen-bonded networks with surface silanol groups with desorption energies of the order of 40 to 70 kJ mol^{-1},[5] the 58 kJ mol^{-1} energy barrier required for reaction R4a to take place may be related to the rupture of the hydrogen-bond network in the activated complex.

Taking the estimated activation energies, assuming $k_4 \approx k_{4a}$ at 298 K, and considering eq 3, the values 1.5×10^{14}, $<1 \times 10^{11}$ and $<1 \times 10^3$ s^{-1} are obtained for the preexponential factors of reactions R4a, R4bg, and R4bs, respectively. Therefore, reactions R4bg and R4bs are less than 10% efficient than reaction R4a, in agreement with the experimental results showing no decrease in the $NPS^\bullet$ decay rate constant at pH < 5.4 where no $SiO^\bullet$ surface radicals are formed. The fraction of undissociated silanols increases considerably below pH 6 (vide supra) favoring water adsorption through an H-bonding network. We may thus expect slightly higher decay rates at the lower pH, as observed experimentally.

To test the proposed reaction mechanism which accounts for the experimental results, a detailed kinetic analysis was performed with the aid of computer simulations (for details of the program see Experimental Section). To this purpose, reactions R1−R3, R4a, R4bg, and R4bs, along with the reactions of $SO_4^{\bullet-}$ radicals with water, hydroxyl ions, and peroxodisulfate ions and $SO_4^{\bullet-}$ bimolecular recombination,[28] were taken into account. The flash emission is considered a Δ function producing $SO_4^{\bullet-}$ radicals. Initial $[SO_4^{\bullet-}]$ taken as an input parameter, was estimated from experiments under identical conditions but in the absence of NP ($\epsilon^{450}(SO_4^{\bullet-}) = 1600$ M^{-1} cm^{-1} [31]), as shown in Figure 1 for experiments c and d. The $NPS^\bullet$ and $SiO^\bullet$ radicals are the only species absorbing at 320 and 600 nm, respectively. Simulated concentration profiles for these transients were converted into the corresponding absorbance curves and compared with the experimental data. An excellent agreement between experimental and simulated profiles is observed taking $\epsilon^{320}(NPS^\bullet) = 7000 \pm 1000$ M^{-1} cm^{-1} and $\epsilon^{600}(SiO^\bullet) \geq 2100 \pm 500$ M^{-1} cm^{-1} (see the solid traces in Figure 1). The lower limit in $\epsilon^{600}(SiO^\bullet)$ values is due to the higher limit values input for reaction rate constants k_{4bg} and k_{4bs}.

We may therefore deduce that the proposed mechanism and estimated reaction rates may account for the observed experimental data.

Conclusion

Sulfate radicals are adsorbed on the NP surface leading to the formation of an adduct with $\lambda_{max} \approx 320$ nm ($\epsilon \approx 7000$ cm^{-1} M^{-1}) and showing reactivity similar to that observed for sulfate radical in aqueous solutions. Adduct formation is independent of the fraction of dissociated surface silanols and showed small adsorption energies. Surface reactions of sulfate radical adducts with adsorbed water and dissociated silanols were observed and the reaction rate constants and their activation energies determined. Sulfate radical hydrogen abstraction from SiOH groups is of no significance. This observation is in agreement with that reported for gaseous HO· radical adsorption over fused quartz where hydrogen abstraction from silanols is only a secondary factor in HO· radical removal from the surface.[32]

Surface reactions of adsorbed sulfate radicals with single and geminal SiO^- yield $SiO^\bullet$ radicals with very similar spectroscopic properties but different reactivity. The observed absorption with $\lambda_{max} \approx 600$ nm is in agreement with that reported for nonbridging oxygen hole centers[29] and for aqueous solutions of $SiO_3^{\bullet-}$ radicals.[30] $SiO^\bullet$ surface radicals formed from geminal SiO^- sites are more reactive than single ones and their reactivity toward ethanol resembles that of $SiO_3^{\bullet-}$ radicals in aqueous solutions.[30]

Formation and decay of adsorbed sulfate radicals on colloidal silica may lead to surface modification, and therefore, the results obtained here are of relevance in those areas involving silica/liquid interface chemistry, as environmental chemistry and catalysis. It is of interest to investigate whether formation of $SiO^\bullet$ surface defects also takes place from the interaction of silica NP with other oxidizing radicals. Experiments to address this question are presently underway.

Acknowledgment. This research was supported by Agencia Nacional de Promoción Científica y Tecnológica, Argentina (ANPCyT) and Consejo Nacional de Investigaciones Científicas y Técnicas, Argentina (CONICET), Fundação de Ampara à Pesquisa do Estado de São Paulo, Brasil (FAPESP) and Fundación Antorchas, Argentina. M.C.G. is a research member of CONICET. D.O.M. is a research member of Comisión de Investigaciones Científicas de la Provincia de Buenos Aires (CIC). P.C. thanks ANPCyT for a graduate studentship.

References and Notes

(1) Conner, W. C.; Pajonk, G. M.; Teichner, S. *J. Adv. Catal.* **1986**, *34*, 1.
(2) (*a*) Brandt, C.; van Eldik, R. *Chem. Rev.* **1995**, *95*, 119;. (*b*) Jury, W. A.; Gardner, W. R.; Gardner, W. H. *Soil Physics*, 5th ed.; Wiley: New York, 1991.
(3) Tripp, C. P.; Hair, M. L. *Langmuir* **1993**, *9*, 3523.
(4) Tripp, C. P.; Hair, M. L. *Langmuir* **1991**, *7*, 923.
(5) Zhuralev, L. T. *Colloids Surf. A: Physicochem. Eng. Aspects* **2000**, *173*, 1.
(6) Vidal, A.; Papirer, E. Chemical reactivity. In *The surface properties of silica*; Legrand, A. P., Ed.; John Wiley & Sons Ltd.: New York, 1998.
(7) Iler, R. K. *The chemistry of silica*; Wiley: New York, 1979; p 623.
(8) Maciel, G. E.; Sindorf, D. W. *J. Am. Chem. Soc.* **1980**, *102*, 7606.
(9) Morrow, B. A.; Gay, I. D. *J. Phys. Chem.* **1988**, *92*, 5569.
(10) Tuel, A.; Hommel, H.; Legrand, A. P.; Sz. Kovats, E. *Langmuir* **1990**, *6*, 770.
(11) van Roosmalen, A. J.; Mol, J. C. *J. Phys. Chem.* **1978**, *82*, 2748.
(12) Allen, L. H.; Matijevic, E. *J. Colloid Interface Sci.* **1969**, *31*, 287.
(13) Allen, L. H.; Matijevic, E. *J. Colloid Interface Sci.* **1970**, *33*, 420.
(14) Allen, L. H.; Matijevic, E.; Meites, L. *J. Inorg. Nucl. Chem.* **1971**, *33*, 1293.
(15) Ong, S.; Zhao, X.; Eisenthal, K. B. *Chem. Phys. Lett.* **1992**, *191*, 327.
(16) Vance, F. W.; Lemon, B. I.; Ekoff, J. A.; Hupp, J. T. *J. Phys. Chem. B* **1998**, *11*, 1845.
(17) Kropp, P. J.; Daus, K. A.; Tubergen, M. W.; Kepler, K. D.; Wilson, V. P.; Craig, S. L.; Baillargeon, M. M.; Breton, G. W. *J. Am. Chem. Soc.* **1993**, *115*, 3071.
(18) Dogliotti, L.; Hayon, E. *J. Phys. Chem.* **1967**, *71*, 2511.

(19) McElroy, W. J.; Waygood, S. J. *J. Chem. Soc., Faraday Trans.* **1990**, *86*, 2557.

(20) Healy, T. W. *Stability of Aqueous Silica Sols in The colloid Chemistry of Silica*; Advances in Chemistry 234; Bergna, H. E., Ed., American Chemical Society: Washington, DC, 1994; p 147.

(21) Mártire, D. O.; Gonzalez, M. C. *Int. J. Chem. Kinet.* **1998**, *30*, 491.

(22) (*a*) Porter, G.; West, M. A. *Techniques of Chemistry*, Hames, G., Ed. Wiley-Interscience: New York. 1974; Vol. VI, Part II, Chapter X. (*b*) Rabek, J. F. *Experimental Methods in Photochemistry and Photophysics, Part I*; John Wiley & Sons: Belfast, Northern Ireland, 1982. Chapter 3.

(23) San Román, E. A.; Aramendía, P. F.; Schumacher, H. J. *An. Asoc. Quím. Argent.* **1980**, *70*, 887.

(24) San Román, E. A.; Gonzalez, M. C. *J. Phys. Chem.* **1989**, *93*, 3532.

(25) Mártire, D. O.; Rosso, J. A.; Bertollotti, S.; Carrillo Le Roux, G.; Braun, A. M.; Gonzalez, M. C. *J. Phys. Chem.* **2001**, *105*, 5385.

(26) (*a*) Choure, S. C.; Bamatraf, M. M. M.; Rao, B. S. M.; Das, R.; Mohan, H.; Mittal, J. P. *J. Phys. Chem. A* **1997**, *101*, 9837. (*b*) Hug, G. L. *Natl. Stand. Ref. Data Ser. (U. S. Natl. Bur. Stand.)* **1981**, 69.

(27) Brusa, M. A.; Churio, M. S.; Grela, M. A.; Bertolotti, S. G.; Previtali, C. M. *Phys. Chem. Chem. Phys.* **2002**, *2*, 2383.

(28) Ross, A. B.; Mallard, W. G.; Helman, W. P.; Buxton, G. V.; Huie, R. E.; Neta, P. *NDRL-NIST Solution Kinetics Database:- Ver. 3.0*; Notre Dame Radiation Laboratory: Notre Dame, IN; National Institute of Standards and Technology: Gaithersburg, MD, 1998.

(29) (*a*) Skuja, L. *J. Non-Cryst. Solids* **1994**, *179*, 51. (*b*) Glinka, Y. D. *Phys. Rev. B* **2000**, *62*, 4733.

(30) Kuzmin, V. A.; Chibisov, A. K. *High Energy Chem.* **1970**, *4*, 146.

(31) McElroy, W. J. *J. Phys. Chem.* **1990**, *94*, 2435.

(32) Suh, M.; Bagus, P. S.; Pak, S.; Rosynek, M. P.; Lunsford, J. H. *J. Phys. Chem.* **2000**, *104*, 2736.